SYNTHESIS OF RANKINITE FROM NATURAL Ca-Si ROCKS AND ITS HARDENING IN CO_2 ATMOSPHERE

AGNE SMIGELSKYTE[1] *, RAIMUNDAS SIAUCIUNAS[1], MATTHIAS WAGNER[2], LIUDVIKAS URBONAS[2]
[1] *Department of Silicate Technology, Kaunas University of Technology, Radvilenu pl. 19, LT–50270 Kaunas, Lithuania*
[2] *Centre for Building Materials (cbm), Technische Universitat Munchen, Baumbachstraße 7, 81245 Munich, Germany*

Rankinite binder material was synthesised from the mixture (C/S = 1.5) of locally (Lithuania) available materials – opoka and limestone – at 1250 °C for 45 min. Its suitability as a non-hydraulic binder for carbonation curing has been assessed. Mortar samples prepared of binder and sand mixture (15:85 wt%, w/c = 0.35) were pressed and cured in a pressure reactor using gaseous (5 and 50 bar at 20 and 50 °C) and supercritical CO_2 (150 bar at 50 °C) for 4 and 24 h. It was determined that with increasing pressure, exposure time and/or temperature the carbonation process is intensified, sample compressive strength is highly increased. Hardening samples at the highest conditions led to full carbonation and the highest strength. For the first time it was shown, that at the supercritical CO_2 conditions the compressive strength of the rankinite binder samples was higher than the OPC ones. The study showed that rankinite as a binder material is suitable for carbonation curing and could be used to produce carbonated construction materials.

Keywords: *Rankinite, non-hydraulic binder, carbonation curing, CO_2, opoka, limestone*

1. Introduction

Ordinary Portland cement (OPC) industry is responsible for 5-7 % of global industrial greenhouse gas emissions [1], therefore, it is important to develop a sustainable alternative to conventional OPC system and to reduce its carbon footprint as much as possible. Above all, one of the most viable options to reduce CO_2 emissions is capture, storage, and sequestration of the emitted CO_2 in the concrete materials [2]. Carbon dioxide capture and storage (CCS) is one of the major areas of interest in the field of recent research studies related to industrial greenhouse gas emission mitigation, where potential storage methods include geological storage, ocean storage, and CO_2 mineralization (i.e. mineral carbonation) [3–5]. Mineral carbonation is a process in which CO_2 is chemically stored in solid inorganic carbonates by carbonation reactions of alkaline materials containing calcium oxides and silicates [4] and includes natural and accelerated processes. Concrete and other cementitious materials absorb CO_2 through a natural process [6]. One of the main consequences of the carbonation reaction of concrete is the modification and reduction of the pH in the pore solution [7]. As a result, conventionally, carbonation reaction of concrete is considered as an unfavourable effect as it decreases the durability performances of such materials [8], moreover, it is also known as a very slow process due to low CO_2 concentration in the atmosphere. Nevertheless, concrete carbonation can have a positive impact on material mechanical properties. Recent research has shown that dry-mix concrete can be treated with carbonation curing at an early age for accelerated strength gain and improved durability [9]. Concrete and OPC carbonation has been widely discussed in the literature [10–17] and is regarded as an opportunity to create a sustainable concrete industry by storing CO_2 in cement-based materials and utilizing carbonate binders with low CO_2 footprint.

However, OPC has a high C/S ratio, since it is mainly composed of lime-rich calcium silicates such as alite and belite, which contribute to CO_2 emissions in the kiln processes. Therefore, an additional way to achieve lower CO_2 emissions and energy consumption is to decrease cement C/S ratio by using low-lime calcium silicates such as rankinite ($3CaO{\cdot}2SiO_2$ or C_3S_2) [18, 19], wollastonite and pseudowollastonite ($CaO{\cdot}SiO_2$ or CS) [19–22] or α-C_2SH [23]. Amounts of limestone required to produce these low-lime calcium silicates are lower than those of OPC and, hence, also contribute to the reduction of the CO_2 emissions

* Autor corespondent/*Corresponding author*,
E-mail: agne.smigelskyte@ktu.edu

from the calcination process involved in the cement production [24]. Moreover, these materials not only contain a lower amount of lime, they also have lower production temperature, which contributes to lower CO_2 emissions as well. However, unlike conventional hydraulic calcium silicates, rankinite is a non-hydraulic binder material and one of the ways to activate and harden it is carbonation curing [20]. These binder systems can store a substantial amount of CO_2 through the hardening process.

Rankinite can be produced from the same calcareous and siliceous raw materials as OPC and its manufacture requires neither specialised equipment nor additional unit operations, and existing OPC plants can be used without almost any modification. Since the temperature of rankinite calcination is about 200 °C [19, 25–27] lower than that of OPC, alternative fuels of lower calorific value can be used for its production. The absence of C_3S in this type of cement makes it less sensitive to cooling rate, therefore rapid cooling is not necessary and the heat losses from the cooler can be considerably reduced. Additionally, the non-hydraulic nature of rankinite eliminates the usage of gypsum as a set-controlling component and since it is not prone to hydration, no special storage arrangements are needed. Moreover, the carbonation curing of rankinite is a relatively speedy process. It can be conducted at ambient pressures and at moderate temperatures of 20 to 60 °C and the concrete products can be cured within a 24-hour period, which makes this process more productive and efficient compared to a 28-day curing cycle required for OPC based concretes [18, 20]. Above all, rankinite curing via a reaction with CO_2 (Eq. 1) provides the possibility for the permanent sequestration of CO_2 in the cured concrete structure. Even though the topic is comparatively relevant, the literature on it is rather scarce, specifically considering rankinite curing via reaction with supercritical CO_2.

$$5(3CaO \cdot 2SiO_2) + 11CO_2 + 2.5H_2O \rightarrow 11CaCO_3 + 4CaO \cdot 10SiO_2 \cdot 2.5H_2O \quad (1)[18]$$

Furthermore, the properties and quality of the raw materials determine the duration and temperature of rankinite synthesis reactions. The use of natural rocks, containing calcium and silicate compounds, as initial materials is recommended since there would be no need to prepare them separately and homogenise afterwards. One of such materials is opoka, a silica-calcite sedimentary rock, found in south-eastern Europe and Russia [28].

Due to the aforementioned reasons, the main purpose of this work was to synthesise rankinite from the locally available materials and to determine carbonation curing condition (gaseous and supercritical CO_2 pressure, exposure time and temperature) impact on its reactivity, reaction products, resulting microstructure, and mechanical properties.

2. Methods and materials

2.1. Characterisation methods

XRD analysis

The crystalline mineral phases were analysed with X-ray diffraction analysis, which was performed on the D8 Advance diffractometer (Bruker AXS) operating at the tube voltage of 40 kV and tube current of 40 mA. The X-ray beam was filtered with Ni 0.02-mm filter to select the Cu-Kα wavelength. Diffraction patterns were recorded in a Bragg–Brentano geometry using a fast counting detector Bruker LynxEye based on silicon strip technology. The specimens were scanned over the range 2θ = 3–70° at a scanning speed of 6° min^{-1} using a coupled two theta/theta scan type. For Rietveld refinement, 10% of ZnO was added as an internal standard for the quantitative determination of the amorphous phase. The samples for XRD analysis were dried at 40 °C for 24 h and ground to < 32 μm.

Mercury intrusion porosimetry

The porosity and pore size distribution of the samples were determined using mercury intrusion porosimetry (AutoPore III, Micromeritics). Isopropanol was used to stop the carbonation reactions of the sample fragments remaining from the strength measurements. From each batch at least two samples from the middle part were taken for the investigation.

Thermal analysis

Simultaneous thermal analysis (thermogravimetric analysis – TG and differential scanning calorimetry – DSC) of the samples was carried out by Netzsch STA 449F3 instrument and analysed between 25 and 1100 °C at the heating rate of 20 K/min under air atmosphere. The samples for thermal analysis were dried at 40 °C for 24 h.

Scanning electron microscopy

The microstructures of the synthesised and carbonated rankinite binder samples were observed using scanning electron microscopy (SEM) (Model JSM-7600F, JEOL Co., Japan) coupled with energy dispersive X-ray spectrometry (EDX) (Inca Energy 350, Oxford Instruments, Silicon Drift type detector X-Max20) was performed by using accelerated voltage of 10kV, the working distance of 8.6 and 8.7 mm for SEM observation, and 200 s accumulation time for EDX analysis. The samples were affixed to the SEM specimen holder using an epoxy resin and then sputter coated with gold to promote electrical conductivity; at least 10 fields of view were analysed for each sample.

Fourier transform infrared spectroscopy

FT-IR spectra have been carried out with the

Table 1

Chemical composition of the raw materials

Oxide, %	SiO_2	Al_2O_3	Fe_2O_3	CaO	MgO	SO_3	K_2O	Other	Ignition loss
Opoka	52.56	2.42	0.78	22.64	0.61	0.45	0.62	0.95	18.97
Limestone	4.38	0.22	0.70	50.88	1.67	0.53	-	-	41.62

Table 2

Chemical and mineralogical composition of C_3S_2 binder, wt.%

Oxide	SiO_2	CaO	Na_2O	K_2O	MgO	Al_2O_3	Fe_2O_3	SO_3	Other
%	42.49	49.48	0.21	0.62	2.79	2.34	1.28	0.20	0.59
Mineral	Rankinite	Akermanite		Bredigite		Pseudowollastonite		Amorphous phase	
%	39	13		2		2		44	

spectrometer Perkin Elmer FT-IR system Spectrum X. Specimens were prepared by mixing 1 mg of the sample material in 200 mg of KBr. The spectral analysis was performed in the range of 4000–400 cm^{-1} with the spectral resolution of 1 cm^{-1}.

Chemical composition

Chemical composition analysis was performed by X-ray fluorescence spectroscopy (XRF) on a Bruker X-ray S8 Tiger WD spectrometer equipped with a Rh tube with the energy of up to 60 keV. Powder samples were measured in Helium atmosphere and data was analysed with SPECTRAPlus QUANT EXPRESS standardless software.

Mechanical properties

The specific surface area of the materials was determined by laser particle size analyser CILAS LD 1090. The density of rankinite was determined using pycnometer AccuPyc 1330 V2.02 (Micromeritics). The compressive strength of the samples was determined according to EN 196-1. The mass and the length of each sample were measured immediately after CO_2 treatment and the residual moisture was determined by drying the grounded samples at the temperature of 40 °C until constant weight.

2.2. Materials and sample preparation

In this work, the following raw materials for rankinite synthesis were used: opoka (Stoniskiu–Zemaitkiemio quarry, Lithuania) and limestone ("Naujasis kalcitas", Lithuania). Both of these materials were dried for 24 h at 100±2 °C and ground in a ball mill (45 rpm, grounding bodies (round, steel) and dry material ratio 1:0.8) for 2 h (opoka specific surface area S = 970 m^2/kg) and 3 h (limestone, specific surface area S = 470 m^2/kg). Chemical composition of the raw materials is shown in Table 1.

A stoichiometric mixture of the raw materials (C/S = 1.5) was homogenised for 2 h at 34 rpm in homogeniser Turbula Type T2F (WAB) and manually granulated into round pellets of ~15–20 mm diameter using a small amount of distilled water. Pellets were dried at 100 °C for 24 h and calcined at a temperature range of 900–1275 °C in a laboratory kiln Nabertherm LHT 08/16. During all calcination experiments, the temperature regime was as follows: the temperature was increased by 10 °C/min up to 850 °C, after 30 min of isothermal treatment, the temperature increase continued to the maximum and the final conditions were maintained for 60 min. After calcination, the pellets were taken out from the kiln at ~ 700 °C, left to cool down to an ambient temperature and ground in a vibratory disc mill Pulverisette 9 (Fritsch) at 900 rpm for 3 min to fine powder <63 μm.

For carbonation curing, the mortar samples were prepared from the following materials: rankinite containing binder, synthesised at 1250 °C for 45 min (specific surface area S = 338 m^2/kg, ρ = 3036 kg/m^3, chemical and mineralogical composition is presented in Table 2); Portland cement CEM I 32.5 R (OPC); CEN standard sand EN-196-1.

Mortar samples were prepared by mixing C_3S_2 or OPC (for comparison with the most widely used binding material) with sand (15:85 wt.%) and adding distilled water; water to cement ratio was 0.35. The samples were pressed in a hydraulic press (pressure – 20 MPa, speed – 2 MPa/s, exposure at maximum pressure – 10 s) to form 50×50 (±0.1) mm cylinders; 205±0.01 g of the mixture was used to make one sample. After the formation, the pressed samples, together with a sample of moist (w/c = 0.35) rankinite binder powder without sand (in order to make a more precise estimation of the newly formed compounds), used for instrumental analysis, were directly transported to the reactor. The samples were treated in the pressure reactor under different conditions: with gaseous CO_2 at 5 and 50 bar, at 20 and 50 °C for 4 and 24 h; with supercritical (SC) CO_2 at 150 bar at 50 °C for 4h and 100 bar at 50 °C for 24h. In the course of all experiments, the pressure was increased and decreased by 2.5 bar/min.

3. Results and discussion

3.1. Rankinite synthesis

The X-ray diffraction analysis was carried out to determine the mineralogical composition of

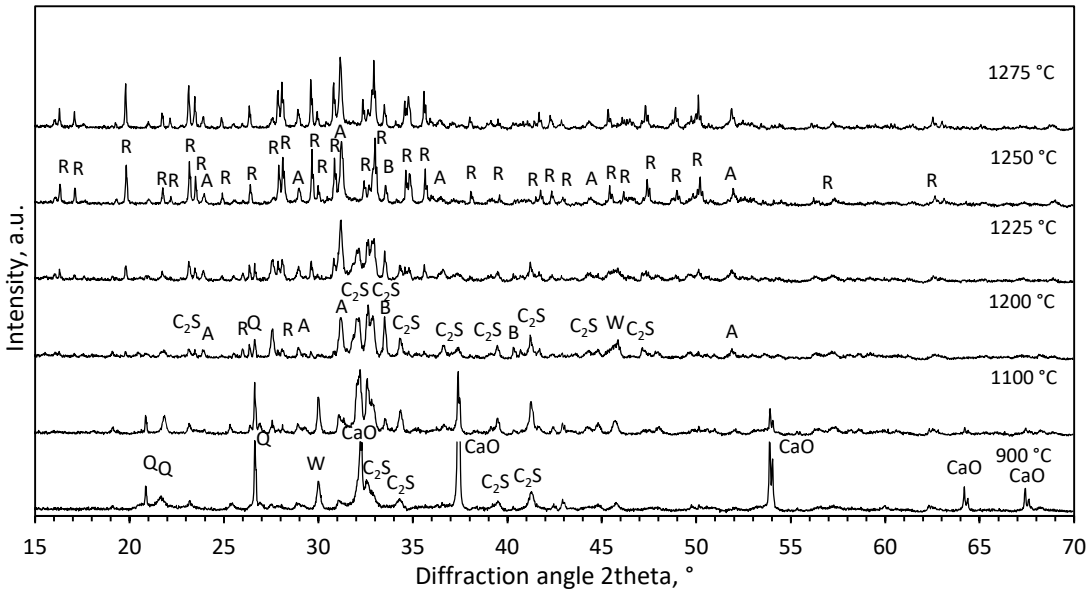

Fig. 1 - X-ray diffraction patterns of pellets exposed to different temperature. Indexes: Q – quartz, W – wollastonite, A – akermanite, B – bredigite, R – rankinite.

the calcined material (Fig. 1) to define the temperature at which rankinite completes the dominant phase. After calcining the material at 900 and 1000 °C, wollastonite and β-C_2S starts to form, however, the main phases are unreacted CaO and quartz. Increasing the temperature up to 1200 °C, the peaks typical to CaO diminish together with quartz, while the amounts of CS and β-C_2S narrowly but coherently increase. Due to a relatively high amount of magnesium in the raw materials, the formation of Ca, Mg silicates such as akermanite and bredigite occurs as well. The rankinite synthesis starts to develop at around 1200 °C and continues to grow with increasing temperature, while the amount of β-C_2S continuously decreases. At the temperature of 1250 °C, the material is mainly composed of rankinite and Ca, Mg silicates (akermanite and bredigite). The further increase of the temperature had no major influence on the phases, intensity, and composition, therefore, it can be concluded that 1250 °C is the optimal temperature for the rankinite synthesis from the raw materials used. The experiments at 1250 °C were extended to find the optimum exposure time. For this reason, the experiments were repeated with the different exposure time from 15 to 60 min. The maximum amount of rankinite was determined in the samples calcined for 45 min and since there was no difference with the 60 min calcination, consequently, the optimum conditions determined for rankinite synthesis are 1250 °C and 45 min. On the other hand, a considerable amount of the amorphous phase remains in the sample (Table 2). Scanning electron microscopy was carried out to determine the prevailing morphology of the formed rankinite. According to the obtained SEM images (Fig. 2), the rankinite is more crystalline and covered in lower amounts of amorphous phase when increasing the calcination duration. However, the rankinite crystals are characterised by an irregular structure, while the amorphous phase was observed to form as a rim of small < 1 μm dispersed fraction on and between calcium silicate grains.

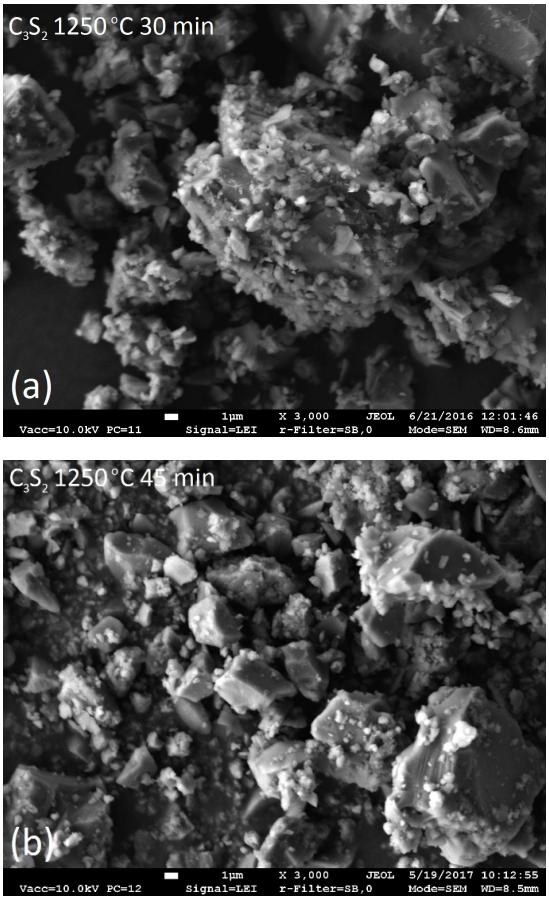

Fig. 2 - SEM micrographs of rankinite binder calcined at 1250 °C for 30 and 45 min.

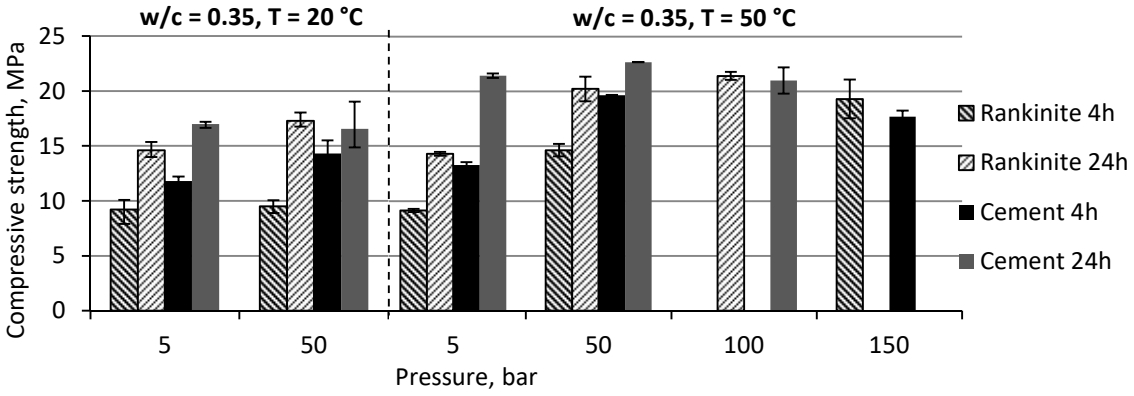

Fig. 3 - Compressive strength of C_3S_2 binder and OPC samples carbonated under different conditions.

3.2. Compressive strength of carbonated samples

CO_2 treatment had a positive influence on the sample hardening process, both C_3S_2 and OPC samples gained a considerably high strength during a relatively short time. By increasing the carbonation pressure and duration, the compressive strength of the samples increased as well (Fig.3).

Although there was no significant difference between samples carbonated at 5 and 50 bar (20 °C), increasing the carbonation temperature from 20 to 50 °C (at 5 and 50 bar), the effect on the sample strength was different, comparing OPC and rankinite samples. The increased temperature had no effect on rankinite samples carbonated at 5 bar for 4 h as well as 24 h, but improved OPC sample strength by about 1.5 MPa on 4 h and 4.5 MPa at 24 h carbonation. Carbonating samples at 50 bar, the increase of the temperature had influence on both rankinite and OPC samples enhancing their compressive strength by ~ 5 MPa at both exposure times. Carbonating samples at SC conditions (100 and 150 bar, at 50 °C) led to further strength increase; at these conditions, rankinite binder samples gained even higher compressive strength than the OPC ones. Although, the observed variety in individual values of the same series samples was probably due to microcracking caused by volume expansion during the carbonation reaction.

3.3. Porosity and pore size distribution

Since diffusion is the limiting stage during the carbonation curing, it is controlled by the pore system and pore saturation. Carbonation of calcium silicates causes the loss of pore connectivity and shifts the pore size distribution curve towards smaller pore diameters as the porosity changes are caused by the dissolution of cementitious phases [29]. Carbonation significantly affects the transport properties by modifying and densifying the microstructure of concrete. It was determined that sample pore size drops with increasing CO_2 pressure (from 5 to 150 bar), as previously large, open pores fill with calcium carbonate, which has a higher molar volume than the initial components. As a result, the reduction of total pore volume is associated with $CaCO_3$ deposition (Fig. 4). The results show that the pore volumes were lower as the carbonation duration and pressure increased. The reduction of pore volume lower than 1 μm indicated the formation of a $CaCO_3$ coating in the carbonation layer, which was also related to the compressive strength development. However, not all changes were significant since the total porosity decreased from 24.5 to 21.3 % when increasing the pressure from 5 to 150 bar.

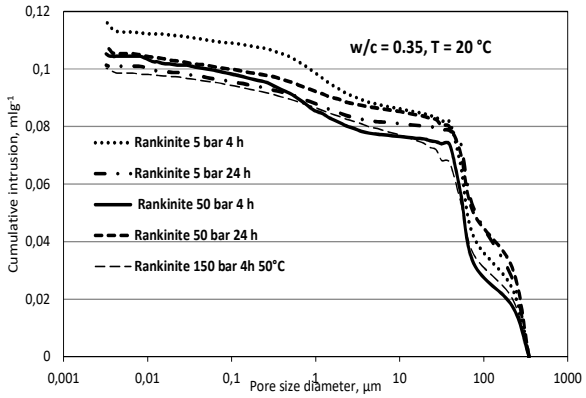

Fig. 4- Pressed C_3S_2 binder sample porosity at different pressure and duration conditions

3.4. Mineralogical observations

Significantly, there were some differences between wet powder and pressed mortar sample mineralogical composition. A lower carbonation degree and a higher amount of rankinite remaining in powder samples (Table 3) could be explained by the fact that in pressed mortar samples quartz may act as a crystalline substrate for calcite formation since both of minerals belong to the trigonal crystal system. Taking into consideration carbonation process, which is strongly exothermic and accelerates water evaporation, other possible

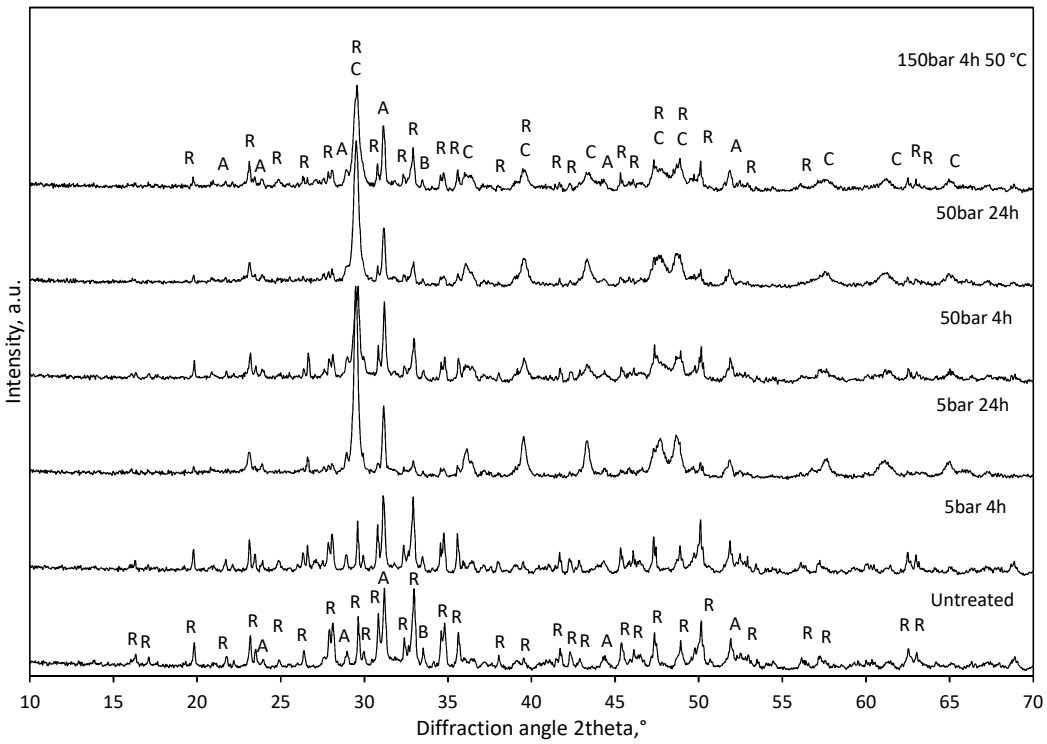

Fig. 5 - X-ray diffraction patterns of rankinite binder powder samples carbonated under different conditions, w/c=0.35, T = 20 °C; Indexes: R – rankinite, C – calcite, A – akermanite, B – bredigite

Table 3

Rietveld refinement results (wt%) of carbonated rankinite binder pressed and powder samples; T = 20 °C

	Powder samples				Pressed samples				
	5 bar 24 h	50 bar, 4 h	50 bar, 24 h	150 bar, 4 h/50 °C	5 bar, 4 h	5 bar 24 h	50 bar, 4 h	50 bar, 24 h	150 bar, 4 h/50 °C
Bredigite	< 1	<1	< 1	< 1	< 1	2	<1	< 1	< 1
Calcite	36	23	32	29	16	40	30	36	45
Pseudowollastonite	1	2	1	2	4	2	3	3	2
Rankinite	4	14	6	8	11	5	11	2	4
Vaterite	1	1	<1	<1	4	2	<1	1	8
Akermanite	7	8	7	7	8	8	8	6	5
Amorphous phase	50	51	51	53	55	43	45	49	37

explanation could be that water from the loose powder can evaporate quite easily when increasing the pressure or temperature in the reactor. In the densely pressed samples, water is concealed in the pore structure and, therefore, is restricted from diffusion to the surface of the sample.

Even though no water is consumed in the carbonation reaction, in the absence of water CO_2 has no media to dissolve into and therefore is restricted from forming carbonic acid which reacts with calcium silicates and forms dense $CaCO_3$ layer. Water takes part in the solvation and hydration of the carbon dioxide by dissolving the Ca^{2+} ions from the solid that will react to form the $CaCO_3$. Hence, it influences the amount of product generated.

As Fig. 5 shows, pressure and exposure time increase had a significant influence on the sample mineralogical composition. X-ray diffraction patterns show the decrease of the rankinite phase, which is being replaced by the calcite phase. Calcium carbonate, present in two polymorphs calcite and vaterite, was the main compound after carbonation.

The decrease of the peaks typical to Ca,Mg-silicates such as bredigite or akermanite shows that not only rankinite reacts with CO_2, but a formation of $(Ca,Mg)CO_3$ (magnesian calcite) is also possible, however, calcite and magnesian calcite generally show similar 2-theta values and are hard to distinguish by XRD analysis [30]. Thus, it is difficult to determine the actual mineralogical composition.

The XRD patterns were supplemented by Rietveld refinement results (Table 3) which show the increasing amount of calcite and the decrease of rankinite and other crystal phases. In fact, the cementitious material had to be separated from the sand grains in crushed pressed mortar samples, therefore it was not possible to completely avoid the presence of quartz. Due to this fact, the final mineral composition was recalculated by deducting the amount of quartz when evaluating the results.

In pressed samples, the amount of rankinite decreases from 11 to 4 wt%, increasing the pressure from 5 to 150 bar, while the amount of calcite increases from 16 to 45 wt% respectively. As expected, the highest amount of calcite (45 wt%) was reached while carbonating at SC conditions.

3.5. Thermal analysis

DSC and TG patters of carbonated rankinite binder powder samples are presented in Fig. 6. The first endothermic peak (Fig. 6, *a*) centred around 90 °C may be an indication of the presence of water in the samples. The second large endothermic peak around 650–800 °C is attributed to the decomposition of calcium carbonate. The third small exothermic peak at around 900 °C may be related with the formation of calcium silicate from CaO released from $CaCO_3$ decomposition and amorphous SiO_2 from the decomposition of C_3S_2. Since there is no mass loss at this point, according to our own rankinite synthesis results, the formation of calcium silicates starts to develop around 900 °C (Fig. 1). As expected, with the increasing pressure and exposure time, the peaks attributed to $CaCO_3$ are larger and broader and the mass loss increases from ~ 3 to 14 %, which corresponds to Rietveld refinement results,
according to the TG data (Fig. 6, *b*). For example, mass loss in samples carbonated at 50 bar for 4 h is ~ 11 %, which stands for ~ 25 % of $CaCO_3$ and matches the amount of carbonate in Rietveld refinement results in Table 3.

3.6. FTIR spectroscopic observations

The FTIR analysis was conducted to investigate the structure of the rankinite binder samples carbonated under different conditions. The FTIR spectra (Fig. 7) for silicate compounds usually exhibit a large absorption between 800 and 1200 cm^{-1}, which corresponds to the asymmetrical stretching vibration of Si–O bond and is visible in all the samples. The absorption bands of calcium silicates below 800 cm^{-1} correspond to the out-of-plate skeletal and in-plate skeletal vibrations of Si–O bond, the band appearing at 470 cm^{-1} is associated with O-Si-O bond bending vibrations. The band at around 1080 cm^{-1} corresponds to vibrations of Si–O bonds present in silica gel phases. According to the literature [18], rankinite has four major absorptions bands located around

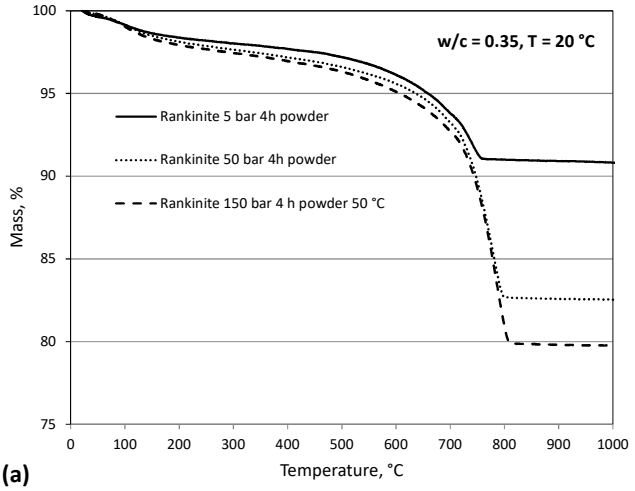

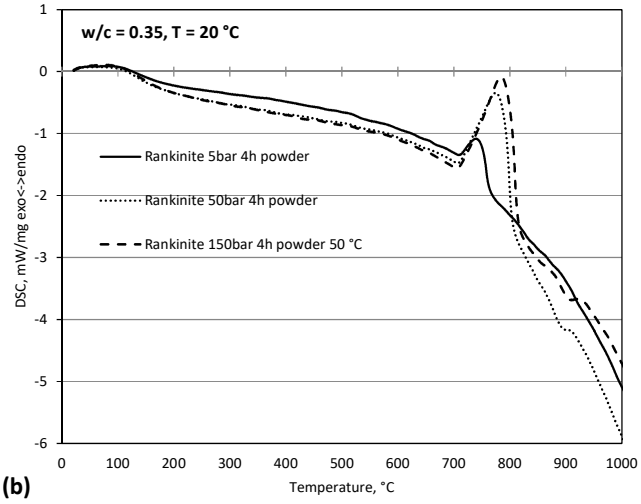

Fig. 6- DSC (*a*) and TG (*b*) curves of carbonated rankinite binder powder samples

846, 906, 940, and 980 cm^{-1} ; in our case, these bands are visible at around 852, 908, 941 and 987 cm^{-1} (Fig. 7).

The characteristic bands of calcite can be found at 1421, 874 and 713 cm^{-1} and all three are present in all carbonated samples. The band located at around 1430 cm^{-1} is due to the asymmetric stretching of Ca–O bond present in $CaCO_3$ and the band located at around 876 cm^{-1} corresponds to the out-of-plane bending vibration of the same C–O bond. The increase in intensity of these bands after carbonation is related with the precipitation of $CaCO_3$ [31].

3.7. Morphological observations

SEM images were collected from the carbonated calcium silicate samples at all conditions. During the carbonation reaction, C_3S_2 initially formed $CaCO_3$ and amorphous SiO_2 phase. At the beginning of the carbonation, rankinite crystals remain considerably large (Fig. 8, *a*) and the crystals of $CaCO_3$ appear to be intermingled with amorphous phase and cover the

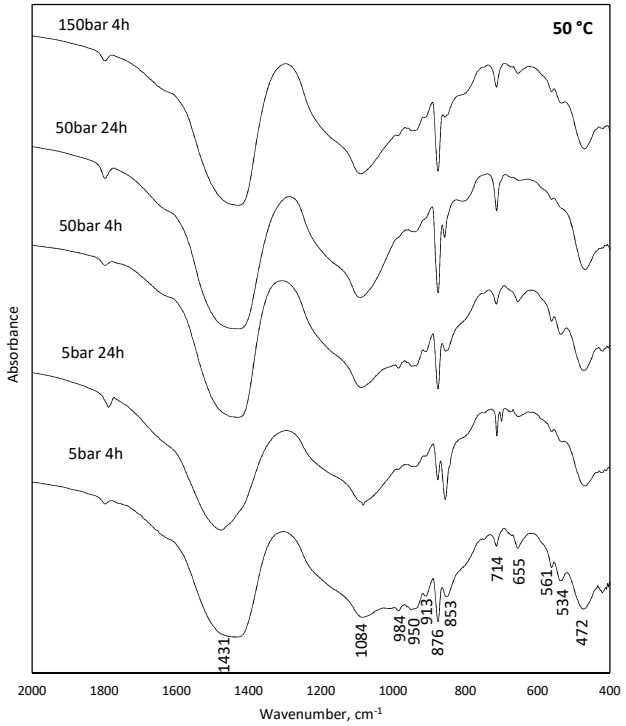

Fig. 7 - FTIR spectra of rankinite binder samples carbonated under different conditions

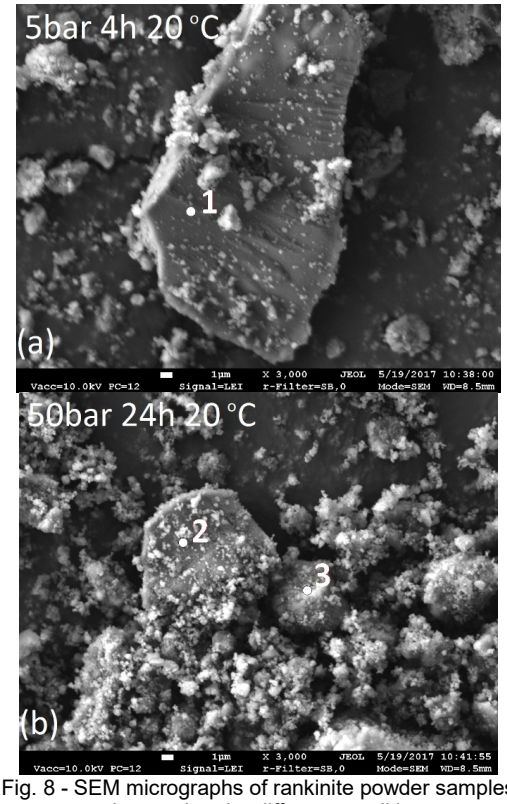

Fig. 8 - SEM micrographs of rankinite powder samples carbonated under different conditions

Table 4

EDX analysis of points 1-3

	Element	C	O	Si	Ca	Total
Point 1	Amount, wt%	-	31.2	22.2	46.6	100
Point 2		6.2	42.6	18.3	32.9	100
Point 3		8.7	53.5	12.8	25	100

large crystals of rankinite. Increasing the carbonation conditions, the crystals of C_3S_2 become considerably smaller and covered in larger amounts of reactions products (Fig. 8, *b*). Amorphous SiO_2 phases were observed covering the unreacted, or partially reacted, C_3S_2 grains with dimensions lower than 1 μm. However, $CaCO_3$ appears to form around rankinite crystals without any specific characteristic dimensions.

Energy dispersive X-ray spectroscopy was performed on a few of the SEM images for approximate determination of the composition of the phases (Fig. 8). Element composition of three points is presented in Table 4. Point 1 on the surface of a large crystal confirms the composition of rankinite and corresponds to carbonating samples under low conditions (5 bar 4 h and 20 °C) led to a low degree of carbonation; the rankinite crystals seem to be unreacted and covered with low amount of other phases. At this point, recalculating elemental to oxide composition, amount of CaO is equal to ~ 65 % and the amount of SiO_2 is ~ 44 %, which leads to molar ratio of C/S ≈ 1.55 that is very close to rankinite C/S. Increasing the conditions led to a higher degree of carbonation, which is confirmed by the composition of points 2 and 3 showing the appearance of carbon and increasing amount of oxygen, that is related to the formation of calcium carbonate. However, the composition of newly formed phases is unstable, since the amount of Si and C is different.

4. Conclusions

In this paper, the carbonation process of rankinite dependence on various conditions such as pressure, exposure time, and temperature was presented. Finally, the following conclusions can be made:

1. The study showed that opoka, as a locally available material, is suitable for rankinite binder synthesis that later-on could be used for production of carbonated concrete construction materials (e.g. tiles, pavers, bricks, etc.). This process could be an environmentally-friendly approach to reduce carbon footprint as well as to attain sustainable development since rankinite binder can be synthesized at 1250 °C, which is 200 °C lower than OPC clinker production temperature. Furthermore, this could be an economically viable option as rankinite binder

manufacturing requires neither specialised equipment nor additional unit operations, and existing OPC plants could be used without almost any modification.

2. While increasing the CO_2 pressure, especially to SC conditions, exposure time, as well as, temperature, the carbonation process is intensified, sample compressive strength is highly improved. Carbonated rankinite mortar samples showed similar or even greater compressive strength results than OPC. The highest compressive strength – 21.42 MPa – of the rankinite binder system was reached with the super critical carbonation at 100 bar for 24h at 50 °C. However, very similar strength (20.23 MPa) was reached while carbonating the rankinite samples at 50 bar for 24h at 50 °C and was very similar to that reached by the OPC samples (22.67 MPa) at the same conditions. Thus, 50 bar 24 h carbonation at 50 °C can be considered as the most economically viable option with the optimal energy requirement.
3. Carbonation conditions have a considerable influence on the sample mineralogical composition: when increasing the parameters of the process (pressure, temperature and time), more rankinite reacts generating a higher amount of calcium carbonate, which is confirmed by the analyses that have been conducted, namely XRD, Rietveld, STA, SEM, FTIR.
4. The importance of moisture should also be emphasised. Water is necessary to promote the reaction of CO_2, however, too much water limits the reaction due to blockage of the pores is the solid material. Hence, further investigations considering different and finding the ideal moisture content should be conducted.

Compliance with Ethical Standards

Conflicts of Interest: The authors declare that they have no conflict of interest.

REFERENCES

1. E. Benhelal, G. Zaheli, E. Shamsaei, A. Bahadori, Global strategies and potentials to curb CO_2 emissions in cement industry, *J Clean Prod,* 2013, **51**, 142-161.
2. J.G. Jang, G.M. Kim, H.J. Kim, H.K. Lee, Review on recent advances in CO_2 utilization and sequestration, *Constr Build Mater,* 2016, **127**, 762-773.
3. L. Kainiemi, S. Eloneva, A. Toikka, J. Levanen, M. Jarvinen, Opportunities and obstacles for CO_2 mineralization: CO_2 mineralization specific frames in the interviews of Finnish carbon capture and storage (CCS) experts, *J Clean Prod,* 2015, **94**, 352-358.
4. D. Xuan, B., Zhan, C.S. Poon, Development of a new generation of eco-friendly concrete blocks by accelerated mineral carbonation, *J Clean Prod,* 2016, **133**, 1235-1241.
5. A. Mazzella, M. Errico, D. Spiga, CO_2 uptake capacity of coal fly ash: Influence of pressure and temperature on direct gas-solid carbonation, *J Environ Chem Eng,* 2016, **4**(4), 4120-4128.
6. T.N. Naik, R. Kumar, R.N. Kraus, Progress Report, Carbon dioxide sequestration in cementitious products. Electric Power Research Institute, Milwaukee, 2009.
7. C.A. Gacia-Gonzalez, N. el Grouh, A. Hidalgo, J. Fraile, A. M. Lopez-Periago, C. Andrade, C. Domingo, New insights on the use of supercritical carbon dioxide for the accelerated carbonation of cement pastes. *J Supercrit Fluid,* 2008, **43**(3), 500-509.
8. W. Ashraf, Carbonation of cement-based materials: Challenges and opportunities, *Constr Build Mater,* 2016, **120,** 558-570.
9. V. Rostami, Y. Shao, A.J. Boyd, Durability of concrete pipes subjected to combined steam and carbonation curing, *Constr Build Mater,* 2011, **25**(8), 3345-3355.
10. D. Zhang, Y Shao, Early age carbonation curing for precast reinforced concretes, *Constr Build Mater,* 2016, **113**, 134-143.
11. M.F. Bertos, S.J.R. Simons, C.D. Hills, P.J. Carey. A review of accelerated carbonation technology in the treatment of cement-based materials and sequestration of CO_2, *J Hazard Mater,* 2004, **112**(3), 193-205.
12. B. Huet, V. Tasoti, I. Khalfallah, A review of Portland cement carbonation mechanisms in CO_2 rich environment, *Enrgy Proced,* 2011, **4**, 5275-5282.
13. A. Leemann, F. Moro, Carbonation of concrete: the role of CO_2 concentration, relative humidity and CO_2 buffer capacity. *Mater Struct,* 2016, **50**(1), 30.
14. I. Galan, C. Andrade, P. Mora, M. A. Sanjuan, Sequestration of CO_2 by Concrete Carbonation, *Environ Sci Technol,* 2010, **44**(8), 3181-3186.
15. M. Mahoutian, Z. Ghouleh, Y. Shao, Synthesis of waste-based carbonation cement, *Mater Struct,* 2016, **49**(11), 4679-4690.
16. S. G. S. Kashef-Haghighi, CO_2 sequestration in concrete thought accelerated carbonation curing in a flow-through reactor, *Ind Eng Chem Res,* 2010, **49**(3), 1143-1149.
17. L. Urbonas, V. Leno, D. Heinz, Effect of carbonation in supercritical CO_2 on the properties of hardened cement paste of different alkalinity *Constr Build Mater,* 2016, **123**, 704-711.
18. W. Ashraf, J. Olek, Carbonation behaviour of hydraulic and non-hydraulic calcium silicates: potential of utilizing low-lime calcium silicates in cement-based materials, *J Mater Sci,* 2016, **51**(13), 6173-6191.
19. S. Sahu, N. DeChristofaro, Solidia Cement, in: Solidia Technol. White Paper. 2013. Online Available: http://solidiatech.com/wp-content/uploads/2014/02/Solidia-Cement-White-Paper-12-17-13-FINAL.pdf. Accessed 17 05 2016.
20. B. Qian, X. Li, X. Shen, Preparation and accelerated carbonation of low temperature sintered clinker with low Ca/Si ratio, *J Clean Prod,* 2016, **120**, 249-259.
21. D. Daval, I. Martinez, J. M. Guigner, R. Hellmann, J. Corvisier, N. Findling, C. Dominici, B. Goffe, F. Guyot, Mechanism of wollastonite carbonation deduced from micro- to nanometer length scale observations, *Am Mineral,* 2009, **94**(11-12), 1707-1726.
22. D. Daval, I Martinez, J. Corvisier, N. Findling, B. Goffe, F. Guyot, Carbonation of Ca-bearing silicates, the case of wollastonite: Experimental investigations and kinetic modelling, *Chem Geol,* 2009, **265**(1-2), 63-78.
23. R. Siauciunas, J. Mikaliunaite, L. Urbonas, K. Baltakys, Tribochemical and thermal activation of α-C_2S hydrate as precursor for cementitious binders, *J Therm Anal Calorim,* 2014, **118**(2), 817-823.
24. W. Ashraf, J. Olek, H. Jeong, V. Atakan, Effects of High Temperature on Carbonated Calcium Silicate Cement (CSC) and Ordinary Portland Cement (OPC) Paste, In *5th International Conference on Durability of Concrete Structures*, Shenzhen, Guangdong Province, P.R. China, 2016.
25. J. Jain, O. Deo, S. Sahu, N. DeChristofaro, Part two of a t series exploring the chemical properties and performance results of Sustainable Solidia Cement™ and Solidia Concrete™, *Solidia Cement,* 2014, 1-16.
26. J.K. Hicks, M. A. Caldarone, E. Bescher, Opportunities from Alternative Cementitious Materials, April 2015. Online Available: https://www.concreteinternational.com. Accessed 26 05 2017.
27. S. Sahu, S. Quinn, V. Atakan, N. DeChristofaro, G. Walenta, CO_2-Reducing Cement Based on Calcium Silicates, in *The 14th International Congress on the Chemistry of Cement*, Beijing, China, 2015.
28. R. Siauciunas, R. Gendvilas, J. Mikaliunaite, L. Urbonas, Application of isomorphic Ca-Si rocks for the synthesis of alpha-C_2S hydrate, *Materials Science/Medziagotyra,* 2014, **20**(3), 321-327.
29. B. Savija, M. Lukovic. Carbonation of cement paste: Understanding, challenges, and opportunities. *Constr Build Mater*, 2016, 117, 285-301.
30. P. De Silva, L. Bucea, V. Sirivivatnanon, Chemical, microstructural and strength development of calcium and magnesium carbonate binders, *Cement Concrete Res,* 2009, **39**(5), 460-465.
31. A. Hidalgo, C. Domingo, C. Garcia, S. Petit, C. Andrade, C. Alonso, Microstructural changes induced in Portland cement-based materials due to natural and supercritical carbonation, *J Mater Sci*, 2008, **43**(9), 3101-3111.

****